Biophysical Journal
Article

Biophysical Society

Spatially Discordant Repolarization Alternans in the Absence of Conduction Velocity Restitution

Chunli Huang,[1,2] Zhen Song,[1] Julian Landaw,[1] and Zhilin Qu[1,3,*]
[1]Department of Medicine, University of California, Los Angeles, Los Angeles, California; [2]Department of Systems Science, Beijing Normal University, Beijing, China; and [3]Department of Computational Medicine, University of California, Los Angeles, Los Angeles, California

ABSTRACT Spatially discordant alternans (SDA) of action potential duration (APD) has been widely observed in cardiac tissue and is linked to cardiac arrhythmogenesis. Theoretical studies have shown that conduction velocity restitution (CVR) is required for the formation of SDA. However, this theory is not completely supported by experiments, indicating that other mechanisms may exist. In this study, we carried out computer simulations using mathematical models of action potentials to investigate the mechanisms of SDA in cardiac tissue. We show that when CVR is present and engaged, such as fast pacing from one side of the tissue, the spatial pattern of APD in the tissue undergoes either spatially concordant alternans or SDA, independent of initial conditions or tissue heterogeneities. When CVR is not engaged, such as simultaneous pacing of the whole tissue or under normal/slow heart rates, the spatial pattern of APD in the tissue can have multiple solutions, including spatially concordant alternans and different SDA patterns, depending on heterogeneous initial conditions or pre-existing repolarization heterogeneities. In homogeneous tissue, curved nodal lines are not stable, which either evolve into straight lines or disappear. However, in heterogeneous itssue, curved nodal lines can be stable, depending on their initial locations and shapes relative to the structure of the heterogeneity. Therefore, CVR-induced SDA and non-CVR-induced SDA exhibit different dynamical properties, which may be responsible for the different SDA properties observed in experimental studies and arrhythmogenesis in different clinical settings.

SIGNIFICANCE Heterogeneous repolarization, which is a key tissue property promoting lethal ventricular arrhythmias, can be either pre-existing in the heart or induced via dynamical instabilities. Spatially discordant alternans (SDA), in which action potential duration alternates out of phase in neighboring regions, is a type of heterogeneous repolarization that is caused by dynamical instabilities. Previous theoretical studies have shown that conduction velocity restitution (CVR) is required for the formation of SDA, which has been supported by some experimental results. However, other experimental results do not support this mechanism. In this study, we investigate the formation and stability of SDA in the absence of CVR, revealing another mechanism of SDA. Our results provide mechanistic insights into SDA observed in experiments and clinical settings where CVR may not be engaged.

INTRODUCTION

T-wave alternans (TWA) as a precursor of ventricular arrhythmias and sudden cardiac death has been known for more than a century (1–6). Experimental and simulation studies have shown that spatially discordant alternans (SDA) is a potential mechanism linking TWA to arrhythmogenesis (7–13). SDA is a spatiotemporal pattern in cardiac tissue in which the action potential duration (APD) exhibits a long-short-long-short alternating behavior, but the alternating pattern is out of phase (or antiphase) in different regions of the tissue. In other words, although the APD may exhibit a long-short-long-short pattern in one region, the APD in its neighboring region may exhibit a short-long-short-long pattern. When the APD exhibits the same pattern throughout the whole tissue, this pattern is called spatially concordant alternans (SCA). For SDA, at the boundaries of out-of-phase regions, the amplitude of alternans is zero (i.e., no APD alternans), which are called nodes in a one-dimensional (1D) cable, nodal lines in a two-dimensional (2D) tissue, or nodal surfaces in a three-dimensional (3D) tissue. SDA results in large APD gradients, which are prone to conduction block and thus reentry formation, mechanistically linking alternans to arrhythmogenesis (8,9).

Submitted October 9, 2019, and accepted for publication February 6, 2020.
*Correspondence: zqu@mednet.ucla.edu
Editor: Eric Sobie.
https://doi.org/10.1016/j.bpj.2020.02.008

Theoretical studies (9,14,15) have shown that SDA is a result of the interaction of cellular APD alternans and the engagement of conduction velocity (CV) restitution (CVR). CVR is an action potential conduction property in which CV slows down as the diastolic interval (DI) is shorter because of incomplete recovery of the sodium (Na^+) channel (7,9). In this theory, the engagement of CVR is required for SDA formation. In other words, the heart rate needs to be fast enough, or the Na^+ channel recovery is slow enough so that CV changes as DI changes. This theory also implies that the nodal lines of SDA are roughly perpendicular to the direction of conduction and closer to the pacing site for faster pacing rates. These characteristic features have been demonstrated in experiments (16–20), supporting the CVR-induced SDA mechanism. However, there are also experimental observations (20–22) that do not support these features; thus, other mechanisms of SDA must be responsible.

Furthermore, in most simulation and experimental studies, SDA has been shown to occur under fast pacing rates (7–9,14–23). However, in many clinical settings, TWA is usually observed in normal or slow heart rates, such as in patients with long QT syndrome (LQTS) (5,24–26), Brugada syndrome (12,27–32), or heart failure (33,34). An important question arises: can SDA be a mechanism linking TWA to arrhythmogenesis under these clinical settings? At normal or slow heart rates, the Na^+ channel may be completely recovered before the next sinus beat. Thus, no CVR is engaged, and the CVR-induced SDA is not applicable. Therefore, if SDA is still a mechanism linking TWA to ventricular arrhythmias under these clinical settings, mechanisms different from the CVR-induced SDA must be responsible. APD alternans has been widely shown in both experiments and simulations to occur in fast heart rates, caused by steep APD restitution or by aberrant calcium (Ca^{2+}) cycling. SDA formation under these cellular mechanisms of alternans has been well investigated (9,14,16,35). Cellular mechanisms of APD alternans at normal or slow heart rates have also been shown. One such mechanism is alternans induced by transient outward potassium (K^+) current (I_{to}) (12,36,37), which may account for TWA in Brugada syndrome. Another mechanism of APD alternans at slow heart rates is APD alternans induced by early afterdepolarizations (EADs) (36,38–40), which may account for TWA in LQTS or heart failure. Moreover, Ca^{2+}-driven alternans can also occur in a wide range of heart rates (41,42). Whether SDA can form at normal or slow heart rates and how it depends on the cellular mechanisms of APD alternans remain unclear. It will be of great importance to address this question because TWA at normal or slow heart rates is widely observed and known as a precursor of lethal arrhythmias in clinical settings (6,24).

In this study, we used computer simulations to investigate the formation and stability of SDA in cardiac tissue in the absence of CVR, namely, to investigate CVR-independent SDA mechanisms. We carried out simulations in 1D cable and 2D tissue models. Three distinct APD alternans mechanisms were used: 1) fast pacing-induced APD alternans, 2) I_{to}-induced APD alternans, and 3) EAD-induced APD alternans. The reason that we chose these different mechanisms of APD alternans is that they occur at different heart rates so that one can choose different heart rates to engage or disengage CVR. We also used two pacing protocols to engage or disengage CVR: one-end pacing and global pacing. CVR is engaged in the one-end pacing when the pacing rate is fast but not engaged when the pacing rate is slow. CVR is absent in the global pacing at any pacing rate because no conduction occurs in this protocol. Our simulations show that SDA can form in the absence of CVR, depending on heterogeneous initial conditions or pre-existing heterogeneous repolarization properties. This mechanism of SDA exhibits dynamical features very different from CVR-induced SDA. It may be a candidate mechanism for the SDA observed in experimental studies that cannot be explained by CVR-induced SDA and provide a potential mechanism linking TWA to arrhythmogenesis in normal or slow heart rates at which CVR is not engaged.

METHODS

Computational models

Computer simulations were carried out in 1D cable and 2D tissue models. The governing partial differential equation for voltage (V) in the 1D cable is as follows:

$$\frac{\partial V}{\partial t} = -\frac{I_{ion} + I_{stim}}{C_m} + D\frac{\partial^2 V}{\partial x^2}, \tag{1}$$

where $C_m = 1\ \mu F/cm^2$, $D = 0.001\ cm^2/ms$, and I_{ion} is the total ionic current density. I_{stim} is the stimulus current density, which is a 2-ms duration and 25-$\mu A/cm^2$ pulse applied periodically with a period called pacing cycle length (PCL). The specific pacing protocols used in this study are described below. An isotropic 2D tissue model was used with the following partial differential equation for V as follows:

$$\frac{\partial V}{\partial t} = -\frac{I_{ion} + I_{stim}}{C_m} + D\left(\frac{\partial^2 V}{\partial x^2} + \frac{\partial^2 V}{\partial y^2}\right). \tag{2}$$

In this study, we mainly used the 1991 Luo and Rudy (LR1) model (43) to demonstrate the underlying mechanisms of SDA. We also used the rabbit ventricular action potential model by Mahajan et al. (44) for an additional demonstration of these mechanisms. A forward Euler method with $\Delta x = \Delta y = 0.0125$ cm and $\Delta t = 0.01$ ms was used for numerical integration of the models. The 1D cable length is 10 cm and the 2D tissue size is 10 × 10 cm^2, corresponding to 800 computational cells in the 1D cable and 800 × 800 computational cells in the 2D tissue, respectively.

Cellular mechanisms of APD alternans

We modified the LR1 model to give rise to different cellular mechanisms of APD alternans. The first type of APD alternans is fast pacing-induced alternans (Fig. 1 *A*), that is, APD alternans occurs as PCL decreases to a certain value. This mechanism of APD alternans is due to steep APD restitution caused by recovery of the ionic currents. Fast pacing-induced APD

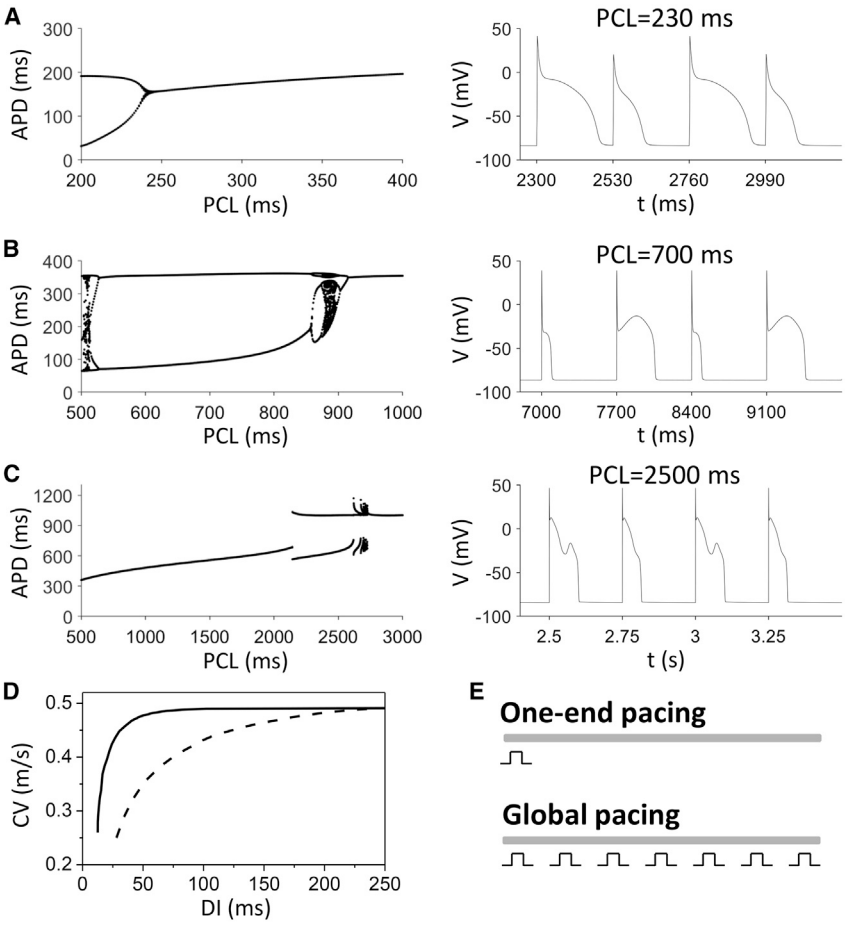

FIGURE 1 Cellular mechanisms of APD alternans in the LR1 model. (*A*) APD alternans caused by fast pacing is shown. The left shows a bifurcation diagram showing APD versus PCL. The right shows a voltage trace showing APD alternans for PCL = 230 ms. Parameters were modified from the original model as follows: $G_{Na} = 16$ mS/cm^2, $G_K = 0.423$ mS/cm^2, $G_{si} = 0.06$ mS/cm^2, and $\tau_j \rightarrow 5\tau_j$. The parameter changes from the original LR1 are to promote cellular APD alternans at fast pacing and to alter CVR to promote SDA in tissue, as shown in our previous study (49). The same parameters were used for Figs. 2, 3, 4, 5, 6, and 7 in this study except for Fig. 2 *C* in which the control τ_j was used. (*B*) I_{to}-induced APD alternans is shown. The left shows a bifurcation diagram showing APD versus PCL. The right shows a voltage trace showing APD alternans for PCL = 700 ms. Parameters were modified from the original LR1 model as follows: $G_{to} = 0.21$ mS/cm^2, $G_{K1} = 1.33034$ mS/cm^2, $G_{si} = 0.1035$ mS/cm^2, and $\tau_x \rightarrow 5\tau_x$, the same parameters as for Fig. 9 in (36). (*C*) EAD-induced APD alternans is shown. The left shows a bifurcation diagram showing APD versus PCL. The right shows a voltage trace showing APD alternans for PCL = 2500 ms. Parameters were modified from the original LR1 model as follows (58): $G_K = 0.25$ mS/cm^2 and $\tau_x \rightarrow 4\tau_x$. (*D*) CVR curves for control τ_j (*solid*) and τ_j that was five times slowed (*dashed*) using the same parameters as in (*A*) are shown. (*E*) Schemes of the two pacing protocols are shown.

alternans has been demonstrated in many experiments and simulations (7–9,16–23,45–48). The parameters that give rise to this mechanism of alternans were set based on our previous study (49), which are described in Fig. 1.

The second type of APD alternans is caused by the presence of I_{to}, which has been investigated in a couple of previous studies (12,36,37,50–54). APD alternans induced by I_{to} can occur in a wide range of heart rates, from fast to normal heart rates (Fig. 1 *B*). This mechanism of alternans may account for TWA in patients with Brugada syndrome (12,27–32). The underlying dynamical mechanism by which I_{to} promotes alternans has been revealed in our previous studies (36,54), in which we developed iterated map models to reveal the bifurcations leading to alternans and chaos. These studies showed that I_{to} unmasked the memory effects caused by other K^+ currents and intracellular ion concentrations to promote APD alternans and chaos at much slower heart rates than in the first mechanism. In this mechanism of alternans, the steep slope of the APD restitution curve is still an important dynamical parameter but not the only determinant for alternans as in the first mechanism. To add this alternans mechanism into the LR1 model, we added I_{to} to the model as described in our previous study (36), with parameter changes described in Fig. 1.

The third type of APD alternans is caused by the occurrence of EADs (Fig. 1 *C*), which has been shown in many previous studies (12,38,39,55–59). This type of alternans, which tends to occur at normal or slow heart rates, may account for TWA in LQTS (39,40). The dynamical mechanism of EAD-mediated APD alternans and chaos was revealed in our previous studies (36,54), which showed that the same iterated map models describing the I_{to}-induced dynamics could well describe the complex dynamics caused by EADs. The parameters for Fig. 1 *C* were set according to our previous study (58), which are described in the Fig. 1 legend.

Altering CVR

We altered CVR by changing the recovery time constant of the Na^+ channel, namely, the time constant (τ_j) of the j-gate. Fig. 1 *D* shows two CVR curves that were used in this study: control τ_j (*solid*) and τ_j that was five times slowed (*dashed*), that is, $\tau_j \rightarrow 5\tau_j$. In the control case, CV varies for DI $<$ 50 ms but remains nearly constant for DI $>$ 50 ms. In the slowed τ_j (or broadened CVR) case, CV varies for DI $<$ 250 ms. The term "CVR engagement" used in this study means that the DI is short enough so that CV changes as DI changes. When the DI is large, CV does not change with DI; thus, there is no CVR engagement.

Heterogeneous initial conditions

Heterogeneous initial conditions were used to induce SDA in certain conditions by setting a spatial distribution of the initial value of a gating variable. We used either the gating variable (x) of the time-dependent K^+ current (I_K) or the gating variable (f) of the slow inward current in the LR1 model. Details of setting the heterogeneous initial conditions are specified in the corresponding figure legends.

Pre-existing repolarization heterogeneities

Pre-existing repolarization heterogeneities were modeled by altering the maximal conductance (G_K) of the I_K in space. Details of the G_K distributions are described in the corresponding figure legends.

Pacing protocols

We used two pacing protocols (Fig. 1 *E*): one-end pacing and global pacing.

In the one-end pacing protocol, the 1D cable or 2D tissue is paced from one side, which results in conduction from the pacing end to the distal end. This pacing protocol corresponds to the conduction in the Purkinje fiber or along the direction of the transmural direction in the heart. CVR is only engaged when the pacing rate is sufficiently fast.

In the global pacing protocol, all the cells in the 1D cable or 2D tissue are paced simultaneously. Because there is no conduction, there is no CVR. In the heart, this pacing protocol corresponds to the excitation of the epicardium. Note that action potentials propagate from the endocardium to the epicardium so that the myocytes in the epicardial layer fire almost simultaneously. In other words, under normal heart rhythms, the conduction in the ventricles is mainly transmural; thus, there is almost no conduction within the epicardial layer (also the endocardial and midmyocardial layers).

RESULTS

CVR-induced SDA under rapid pacing

Although CVR-induced SDA has been investigated in many previous simulation studies (9,14,60), to compare the dynamical properties of CVR-induced SDA and non-CVR-induced SDA, we first carried out simulations of CVR-induced SDA. To engage CVR and thus facilitate the formation of CVR-induced SDA, we used the one-end pacing protocol to allow conduction along the cable and used rapid pacing to engage short DIs (Fig. 1 *A*). Furthermore, the DI range that CV varies was broadened (the broadened CVR curve) by slowing the recovery of the Na^+ channel (Fig. 1 *D*, *dashed line*). Fig. 2 *A* shows SDA induction under this condition with constant period pacing (PCL = 240 ms). A node first formed in the distal end of the cable (at beats 4 and 5), and as time progressed, new nodes gradually formed in the distal end and moved toward the pacing site (Fig. 2 *A*). A total of three stable nodes were formed in this cable. To examine whether the SDA pattern depends on initial conditions (Fig. 2 *B*), instead of using a fixed PCL, we applied a pacing beat from the distal end of the cable after the first pacing beat, representing a premature ventricular complex (PVC). We then resumed the fixed PCL after the PVC propagated through the cable. In this case, a node formed near the pacing end immediately after the PVC beat, but new nodes still formed from the distal end.

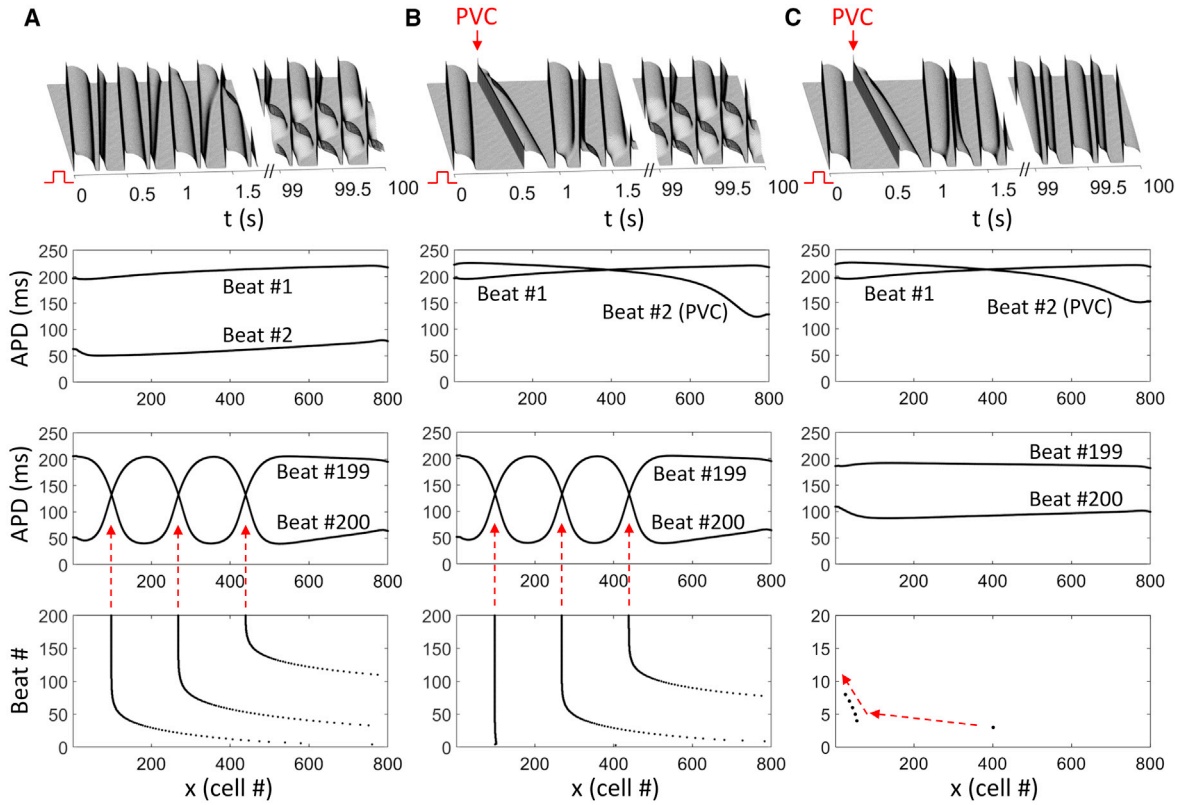

FIGURE 2 SDA induced by CVR in a homogeneous cable. The cable was paced using the one-end pacing protocol. In each case, the top panel is a 3D plot of voltage (time-space-voltage), the second panel shows APD in space for the first two beats, the third panel shows APD in space for the last two beats, and the bottom panel shows the node positions over time. The total number of pacing beats is 200. (*A*) Fixed pacing with PCL = 240 ms was used. (*B*) A PVC was given as the second beat from the other end of the cable (marked by *arrow*) and then fixed pacing with PCL = 240 ms was used. (*C*) The same pacing protocol as in (*B*) is shown, but it avoids CVR engagement by using the control τ_j in the original LR1 model. Note that the arrows between the third panel and the bottom panel in (*A*) and (*B*) link the node positions in two plots. A node is defined as a point in the cable at which the APDs in the two consecutive beats are the same (i.e., $\Delta APD = APD_{n+1} - APD_n = 0$). ΔAPD changes from positive to negative or vice versa across a node. In (*C*), the initial node (at position cell 400) moves off the cable (following the *arrows*) within 10 beats. To see this figure in color, go online.

As time progressed, the same SDA pattern as in Fig. 2 *A* was formed. This indicates that the SDA pattern is stable, independent of initial perturbations. To further examine the role of CVR in the genesis and stability of SDA patterns (Fig. 2 *C*), we used the control Na^+ channel recovery for which the CVR curve has a narrower DI range of varying CV (Fig. 1 *D*, *solid line*) and applied a PVC to induce an SDA node. For PCL = 240 ms, CVR is not engaged (note that as shown in the third panel of Fig. 2 *C*, the APDs in the two alternating beats are ~190 and ~100 ms, which means DI = PCL−APD > 50 ms; therefore, no CVR is engaged). In this case, the PVC-induced node quickly disappears, resulting in SCA. This indicates that in the absence of CVR, an initial-condition-induced SDA node is unstable.

These simulations show that when CVR is engaged, the SDA pattern does not depend on the initial conditions, that is, different initial conditions lead to the same SDA pattern. In other words, the SDA nodes induced by CVR are stable against perturbations. But in the absence of CVR, a heterogeneous initiation-condition (i.e., a PVC)-induced SDA node is unstable. Therefore, CVR is needed to maintain a stable SDA pattern under rapid pacing with conduction in a homogeneous tissue.

CVR-independent SDA under rapid pacing

We then investigated CVR-independent mechanisms of SDA under rapid pacing. To avoid CVR engagement, we paced all the cells in the 1D cable simultaneously (i.e., the global pacing protocol). Under this pacing protocol, there is no conduction and thus no CVR engagement. SDA can be induced by heterogeneous initial conditions, PVCs, or pre-existing heterogeneous repolarization. Note that in the one-end pacing case in Fig. 2, we used PCL = 240 ms, but in the global pacing cases, we used PCL = 230 ms. This is because the PCL onset of alternans is different under the two pacing protocols because of cell coupling and conduction (61).

We first show SDA induced by heterogeneous initial conditions in a homogeneous cable with global pacing (Fig. 3). The heterogeneous initial conditions were set by using heterogeneous distributions of the initial value of f (a gating variable of the slow inward current) as detailed in the legend of Fig. 3. When the initial condition was homogeneous or weakly heterogeneous, SCA occurred (Fig. 3 *A*). However, when the initial condition was strongly heterogeneous, SDA occurred (Fig. 3, *B* and *C*). The resulted SDA pattern depends on the initial condition, and it can exhibit one node (Fig. 3 *B*) or two nodes (Fig. 3 *C*). Once the nodes are formed, they almost do not move (see the node positions shown in Fig. 3, *bottom panels*). In the one-node case, the node position can be anywhere in the cable (Fig. 2 *B*, *solid line* and *dashed line* are two examples) as long as the node is a distance away from the boundary. Because the node can be formed anywhere in the cable, the node stability is neutral or marginal because the nodal position will be changed after a perturbation.

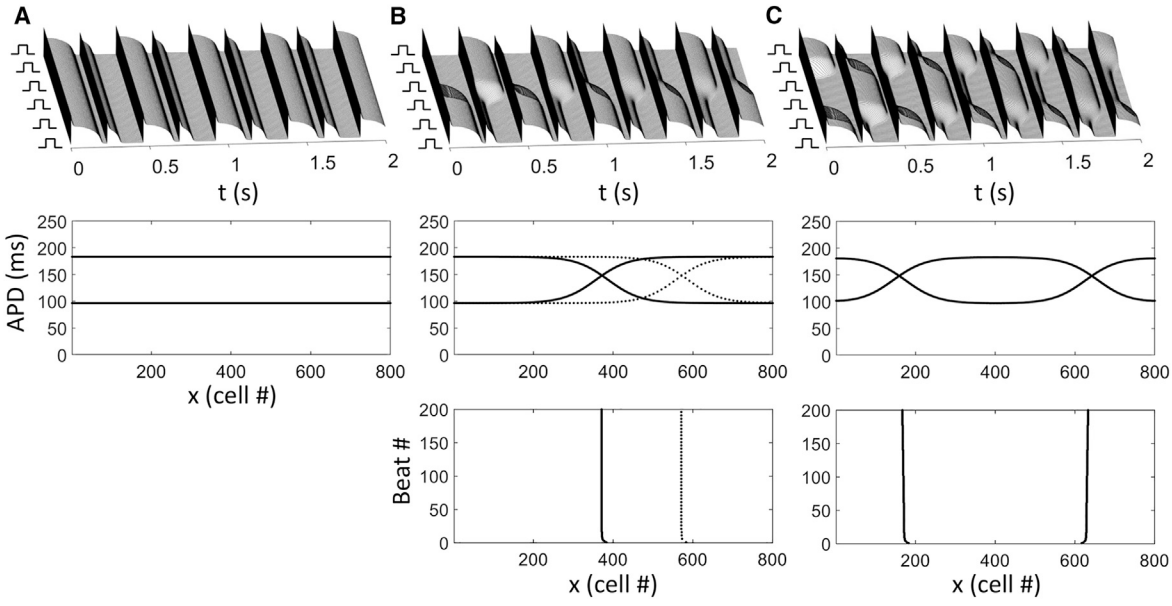

FIGURE 3 Heterogeneous initial-conditions-induced SDA in a homogeneous cable with global pacing. The cable was paced using the global pacing protocol; that is, the cells in the cable were simultaneously paced. PCL = 230 ms. In each case, the top panel is a 3D plot of voltage (time-space-voltage), the middle panel shows APD in space for the last two beats, and the bottom panel shows the node positions over time. The total number of pacing beats is 200. (*A*) A homogeneous initial condition leads to SCA. (*B*) A heterogeneous initial condition leads to a single node. In this case, the initial value of the gating variable f of the slow inward current was set as 1 for the first 400 cells and 0.01 for the next 400 cells for the solid lines. For the dashed lines, the initial value of f was set as 1 for the first 600 cells and 0.01 for the next 200 cells. (*C*) A heterogeneous initial condition leads to two nodes. In this case, the initial value of the gating variable f was set as 1 for the first 200 cells, 0.01 for the next 400 cells, and 1 again for the last 200 cells.

We then show PVC-induced SDA in a homogeneous cable under global pacing (Fig. 4). Fig. 4 *A* shows a single node induced in a homogeneous cable by a PVC starting from one end of the cable. Note that after the PVC, we still used the global pacing protocol; thus, the PVC effectively results in a heterogeneous initial condition for the beat right after it. Fig. 4 *B* shows two nodes induced by PVCs from the two ends of the cable.

To investigate the role of pre-existing repolarization heterogeneities in SDA formation and stability, we carried out simulations in a heterogeneous cable under global pacing with homogeneous initial conditions. The repolarization heterogeneity was modeled by using a smaller G_K (thus, a longer APD) in the right half of the cable compared to the left half. Fig. 5 *A* shows an SCA pattern when the cable was paced with a fixed PCL = 230 ms. The alternans amplitude is larger on the right side of the cable (ΔAPD is ~90 ms on the left end and ~140 ms on the right end). However, when we shortened the pacing interval for one of the pacing beats from 230 to 130 ms (Fig. 5 *B*, marked by the *arrow*), SDA was induced. The reason that one needs to shorten the pacing interval in a beat to induce SDA is likely that the APD gradient is not large enough in this case. Differing from the nodal behaviors in the homogeneous cable, the node shown in Fig. 5 *B* drifted slowly from the APD gradient region to the short APD region. Note that the node was still drifting, albeit slower, at beat 500, and theoretically, it may drift forever as long as there is an APD gradient. This is because the node stability is neutral in a homogeneous cable, and a repolarization gradient may generate a tension for the node to drift.

In this same heterogeneous cable, when paced from one end to engage CVR, an almost identical SDA pattern to the ones shown in Fig. 2 occurred (Fig. 5 *C*). All three nodes were stable after ~150 beats. This indicates that the repolarization heterogeneity has almost no or a very small effect on CVR-induced SDA in this setting.

The simulations shown in Figs. 3, 4, and 5 demonstrate that in the absence of conduction, SDA can be formed via heterogeneous initial conditions, PVCs, or pre-existing repolarization heterogeneities. The SDA node is neutrally stable in a homogeneous cable but may drift in a heterogeneous cable.

SDA formation and nodal line dynamics in 2D tissue

In 2D tissue, the SDA nodes form nodal lines. A question arises: what types of stable nodal lines can exist in 2D tissue when CVR is not present? Here, we address this question using the fast pacing-induced APD alternans (Fig. 1 *A*) and the global pacing protocol to disengage CVR. Our simulations show that in homogeneous 2D tissue, only stable straight nodal lines can exist. Fig. 6 *A* shows an example in which an initially curved nodal line gradually deformed to a straight nodal line (also see Video S1 for the nodal line motion). On the other hand, a nodal ring in homogeneous 2D tissue shrinks continuously until it disappears (Fig. 6 *B*, also see Video S2 for the nodal ring motion). However, in a 2D heterogeneous tissue in which the APD in the center region is longer, the nodal ring shrinks initially but eventually becomes stable (Fig. 6 *C*; Video S3). In the homogeneous case, the area decreases almost linearly to zero (Fig. 6 *D*, *solid line*). This linear relationship also holds for alternans induced by I_{to} and EADs (see results described later). Because the SDA node is neutrally or marginally

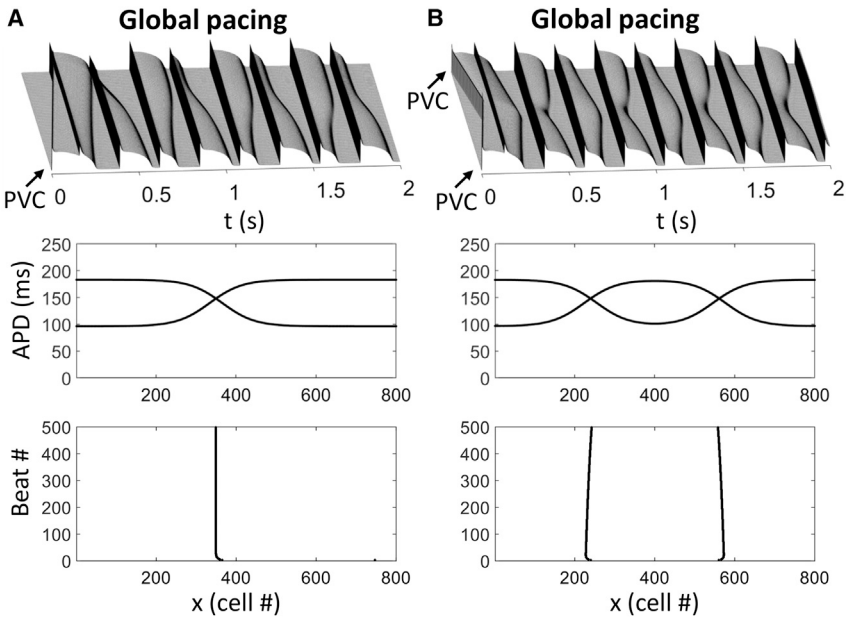

FIGURE 4 PVC-induced SDA in a homogeneous cable with global pacing. The cable was paced using the global pacing protocol with PCL = 230 ms. In each case, the top panel is a 3D plot of voltage (time-space-voltage), the middle panel shows APD in space for the last two beats, and the bottom panel shows the node positions over time. The total number of pacing beats is 500. (*A*) A PVC (*arrow*) from one end to result in one node is shown. (*B*) Two PVCs (*arrows*) from the two ends to give rise to two nodes are shown.

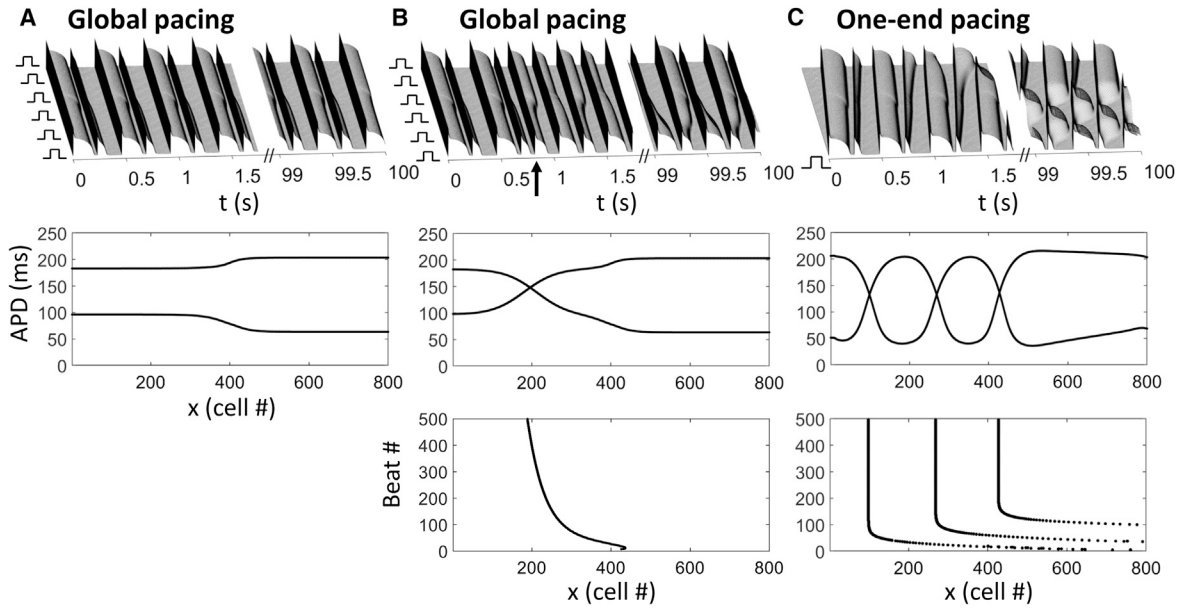

FIGURE 5 Effects of repolarization heterogeneities on SDA formation. The APD heterogeneity was induced by setting $G_K = 0.423$ mS/cm^2 (the control value) in the first 400 cells and 0.38 mS/cm^2 in the next 400 cells. In each case, the top panel is a 3D plot of voltage (time-space-voltage), the middle panel shows APD in space for the last two beats, and the bottom panel shows the node positions over time. The same homogeneous initial condition was used. The total number of pacing beats is 500. (*A*) Global pacing with PCL = 230 ms is shown. (*B*) Global pacing with PCL = 230 is shown, but a shorter interval (130 ms) between the fourth beat and the fifth beat (*arrow*) was applied. (*C*) One-end pacing with PCL = 240 ms is shown.

stable in homogeneous tissue, the curvature of the nodal ring results in a tension that causes the ring to shrink. For the heterogeneous case, as shown in the 1D heterogeneous cable (Fig. 5 *B*), a node formed in the repolarization gradient region drifts toward the short APD region. Therefore, in the case of Fig. 6 *C* in which APD is longer in the central region, the drifting tension generated by the curvature is opposite to the tension generated by the repolarization gradient. The tensions eventually balance with each other to result in a stable nodal ring.

Because of the tensions generated by the repolarization gradient and by the nodal line curvature can be balanced, curved nodal lines can be stable in heterogeneous tissue. The stable nodal ring in Fig. 6 *C* is a special case of a curved nodal line. Fig. 7 *A* shows three scenarios of curved nodal line dynamics in the same heterogeneous tissue. In the first case (Fig. 7 *A*, *left panel*; Video S4), an initially curved nodal line becomes a straight line as if the tissue were homogeneous. In the second case (Fig. 7 *A*, *middle panel*; Video S5), an initially straight nodal line becomes curved and eventually stable at which the tensions from the curvature and repolarization gradient are balanced. In the third case (Fig. 7 *A*, *right panel*; Video S6), an initially straight nodal line becomes curved but drifts toward the tissue border and disappears. Therefore, the nodal line shape and its stability depend on its initial position relative to the heterogeneous region.

However, CVR-induced nodal lines almost do not depend on the heterogeneity. Fig. 7 *B* shows nodal lines in the same heterogeneous tissue above by pacing from one side of the tissue (the one-end pacing protocol). The nodal lines are always perpendicular to the direction of propagation, irrespective of the structure of the heterogeneity.

Therefore, in the absence of conduction, a curved nodal line is unstable in a homogeneous tissue but can be stabilized in heterogeneous tissue because of the competition of the tensions generated by curvature and repolarization gradients.

SDA under normal and slow heart rates

The results shown above are SDA formation and dynamics under fast pacing. We then investigate SDA formation and dynamics in the case of APD alternans caused by I_{to} (Fig. 1 *B*) and by EADs (Fig. 1 *C*) under slow pacing. Under these cases, CVR is not engaged during alternans because DI is large (Fig. 1 *D*, see CVR curves), that is, CV remains constant during the alternating beats.

We first carried out 1D cable and 2D tissue simulations for I_{to}-induced APD alternans at PCL = 700 ms. Fig. 8 *A* shows APD alternans patterns in a homogeneous cable with the global pacing protocol but different initial conditions (different initial values of the gating variable x of I_K as detailed in the legend of Fig. 8). One can induce SCA or multiple-nodes SDA in this same cable, similar to the case of APD alternans induced by fast pacing shown in Fig. 3. In a heterogeneous cable, SDA can be induced and becomes stable by either global pacing or one-end pacing with homogeneous initial conditions (Fig. 8 *B*). Note that in this setting, we do not need to change the pacing interval to induce SDA as in the case shown in Fig. 5 *B*. In the

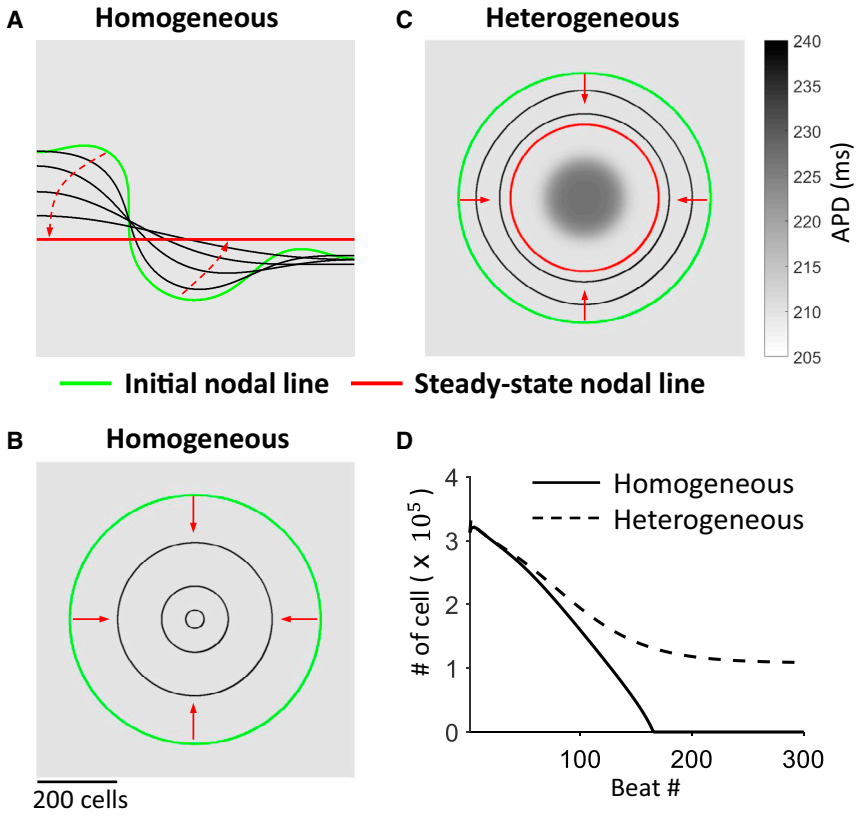

FIGURE 6 Curved nodal line dynamics in 2D tissue. (*A*) Nodal lines at different time points showing an initially curved nodal line evolves into a straight nodal line (from the *green line* to the *red line* indicated by the *dashed arrows*) in a homogeneous tissue (see Video S1 for the nodal line motion). (*B*) Nodal lines at different time points show that a heterogeneous initial-condition-induced nodal ring (*green*) shrinks (indicated by *arrows*) and disappears in a homogeneous tissue (see Video S2 for the nodal ring motion). (*C*) Nodal lines at different time points show that an initial nodal ring (*green*) shrinks (indicated by *arrows*) but becomes stable (*red*) in a heterogeneous tissue (see Video S3 for the nodal ring motion). $G_K = 0.35$ mS/cm^2 in the central region with a radius of 100 cells, which was reduced from the control value ($G_K = 0.423$ mS/cm^2) to increase APD. (*D*) The area (total number of cells) inside the nodal ring versus beat number for the case in (*B*) (*solid line*) and the case in (*C*) (*dashed line*) is shown. Global pacing with PCL = 230 ms is used, and the tissue size is 800 × 800 cells. The grayscale background in each panel is APD under PCL = 500 ms as indicated by the scale bar. The initial nodal line (*green*) was induced by a heterogeneous initial distribution of the gating variable *f* similar to the way in Fig. 3. To see this figure in color, go online.

one-end pacing case, the SDA is not caused by CVR but by the heterogeneity alone. This is because the longest APD is ~350 ms; at PCL = 700 ms, the shortest DI is ~350 ms. In this case, the Na^+ channel is almost 100% recovered at the next pacing beat; thus, no CVR is engaged (we used the control Na^+ channel recovery; Fig. 1 *D*, *solid line*). In other words, CV is almost constant for DI > 350 ms. Therefore, in both cases, the discordance of the APD alternans is induced by the heterogeneity.

We also carried out simulations to investigate the nodal ring dynamics in both homogeneous and heterogeneous 2D tissue. A nodal ring in a homogeneous tissue always shrinks and eventually disappears (Fig. 8 *C*), and the area inside the ring decreases linearly with time (Fig. 8 *E*, *solid line*). On the other hand, a nodal ring can be stabilized in a heterogeneous tissue (Fig. 8, *D* and *E*, *dashed line* in the latter panel) because of the competition of the tensions generated by the curvature and the heterogeneity. Note that in the case shown in Fig. 8 *D*, the nodal ring first expanded and was finally stabilized. Differing from the case showing in Fig. 6 *C*, in which APD is longer in the central region, in the case of Fig. 8 *D*, the APD is shorter in the central region. But in both cases, the heterogeneity generated an expanding tension against the shrinking tension generated by the curvature to stabilize the nodal ring. More rigorous analyses are needed to dissect this difference and reveal the underlying mechanisms.

We then carried out 1D cable and 2D tissue simulations to investigate the SDA dynamics for EAD-induced APD alternans under global pacing (Fig. 9). Fig. 9 *A* shows an SCA induced by a homogeneous initial condition, and Fig. 9 *B* shows an SDA induced by a heterogeneous initial condition in a homogeneous cable. Fig. 9 *C* shows that a heterogeneous initial-condition-induced nodal ring shrinks with time and eventually disappears in a homogeneous 2D tissue. Fig. 9 *D* shows that the area inside the ring decreases linearly with time.

However, in both the I_{to} and EAD cases, when we used one-end pacing, the nodes induced by heterogeneous initial conditions or PVCs are not stable in the homogeneous cable. These nodes always disappear to result in SCA.

These simulations demonstrate that in the absence of conduction, for alternans at normal and slow heart rates, SDA can be induced by heterogeneous initial conditions and pre-existing heterogeneous repolarization. In the presence of conduction without the CVR engagement, the SDA node is unstable in homogeneous tissue, but it can be stabilized in heterogeneous tissue. The SDA dynamics are similar to those for APD alternans induced by rapid pacing.

Formation of SDA in a rabbit ventricular action potential model

The same mechanisms of SDA also hold in other action potential models. Fig. 10 shows SCA and SDA in a rabbit

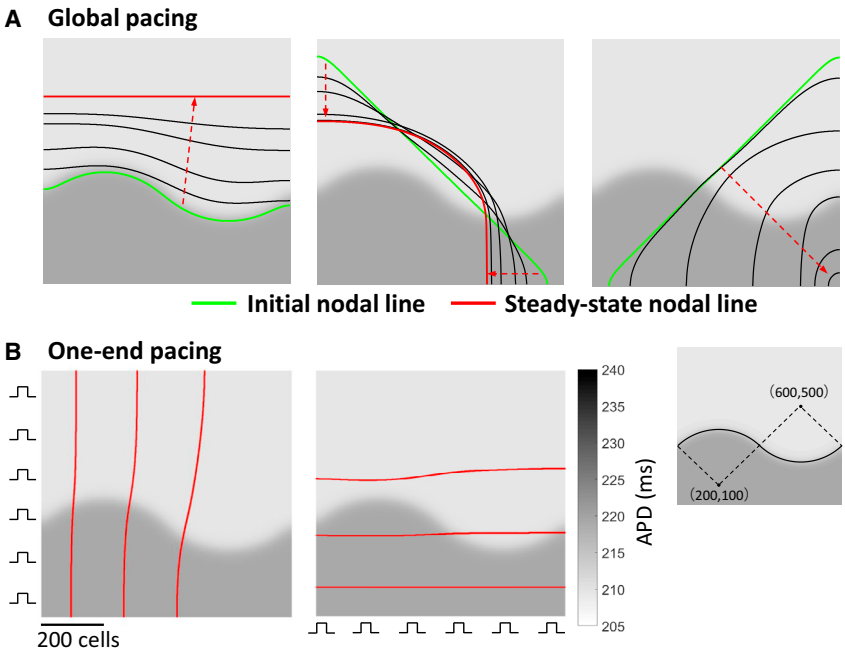

FIGURE 7 Effects of repolarization heterogeneity on curved nodal line dynamics in 2D tissue. (*A*) Different nodal line dynamics due to different initial conditions under global pacing with PCL = 230 ms in the same 2D tissue are shown. Shown are nodal lines at different time points. Green lines are the initial ones induced by heterogeneous initial conditions. The red lines are the final steady state. The left panel shows an initially curved nodal line becoming a straight nodal line (Video S4). The middle panel shows formation of a stable curved nodal line (Video S5). The right panel shows disappearance of a curved nodal line (Video S6). (*B*) Steady-state nodal lines induced by one-end pacing with PCL = 250 ms in the same heterogeneous tissue as in (*A*) are shown. The left panel shows pacing from the left side. The right panel shows pacing from the bottom side. For both (*A*) and (*B*), the heterogeneity was generated by setting G_K = 0.38 mS/cm^2 in the lower part (*dark region*) and the control value (G_K = 0.423 mS/cm^2) in the upper part of the tissue (the inset shows the parameter boundary consisting of two arcs with center coordinates marked). The tissue size is 800 × 800 cells. The grayscale background in each panel is APD under PCL = 500 ms as indicated by the scale bar. To see this figure in color, go online.

ventricular action potential model (44). APD alternans in this model occurs at fast pacing. Under global pacing, both SCA and SDA can be induced in the same homogeneous cable (Fig. 10 *A*). SDA can also be induced by one-end pacing in which CVR is engaged (Fig. 10 *B*). These behaviors are the same as in the LR1 model shown in Figs. 2 and 3.

DISCUSSION

In this study, we use computer simulations to investigate the formation and stability of SDA in the absence of CVR in cardiac tissue models. The simulation results show that under fast pacing in which CVR is present and engaged, the tissue can only exhibit one spatial APD pattern, either SCA or SDA, independent of initial conditions or pre-existing repolarization heterogeneities. Under global pacing or slow heart rates in which CVR is not engaged, the tissue can exhibit multiple spatial APD patterns; that is, SCA and different SDA patterns can occur in the same tissue, depending on heterogeneous initial conditions, PVCs, or pre-existing repolarization heterogeneities. In the latter mechanism of SDA, the nodes or the noncurved nodal lines are marginally stable in homogeneous tissue. Because of this, curved nodal lines are not stable in homogeneous tissue. They either evolve into straight lines or disappear. However, curved nodal lines can be stable in heterogeneous tissue, depending on their initial locations and shapes relative to the structures of the heterogeneities. Together, the CVR-induced SDA and non-CVR-induced SDA can explain the different SDA properties observed in experimental studies. Both mechanisms of SDA may occur in the heart and promote arrhythmias at different clinical conditions as discussed below.

Mechanisms of SDA

Early theoretical studies (7,9,14,15) have shown that the formation of SDA requires the engagement of CVR. The mechanism is as follows. When DI is short (or the heart rate is fast), the Na^+ channels have not completely recovered yet; thus, CV changes as DI changes. Because the DI also alternates during alternans, then CV is different in the alternating beats, which cannot remain constant but changes along the conduction pathway. The change in CV along the conduction pathway causes DI and APD to change during conduction, resulting in SDA (9). When the DI is long (or the heart rate is slow), the Na^+ channels are recovered completely so that CV no longer changes with DI. Although DI alternates during alternans, CV is maximum and remains the same in the alternating beats. Therefore, APD and DI exhibit no change along the conduction pathway as a result of constant CV; thus, no SDA forms. A formal nonlinear dynamics analysis using the amplitude equation approach by Echebarria and Karma (15,62) reveals a spatiotemporal instability leading to SDA. The mechanism of CVR-induced SDA has been demonstrated in experiments (16–20). Other mechanisms of SDA, in particular when alternans is caused by instability of Ca^{2+} cycling, have also been shown in computer simulations (35,63,64).

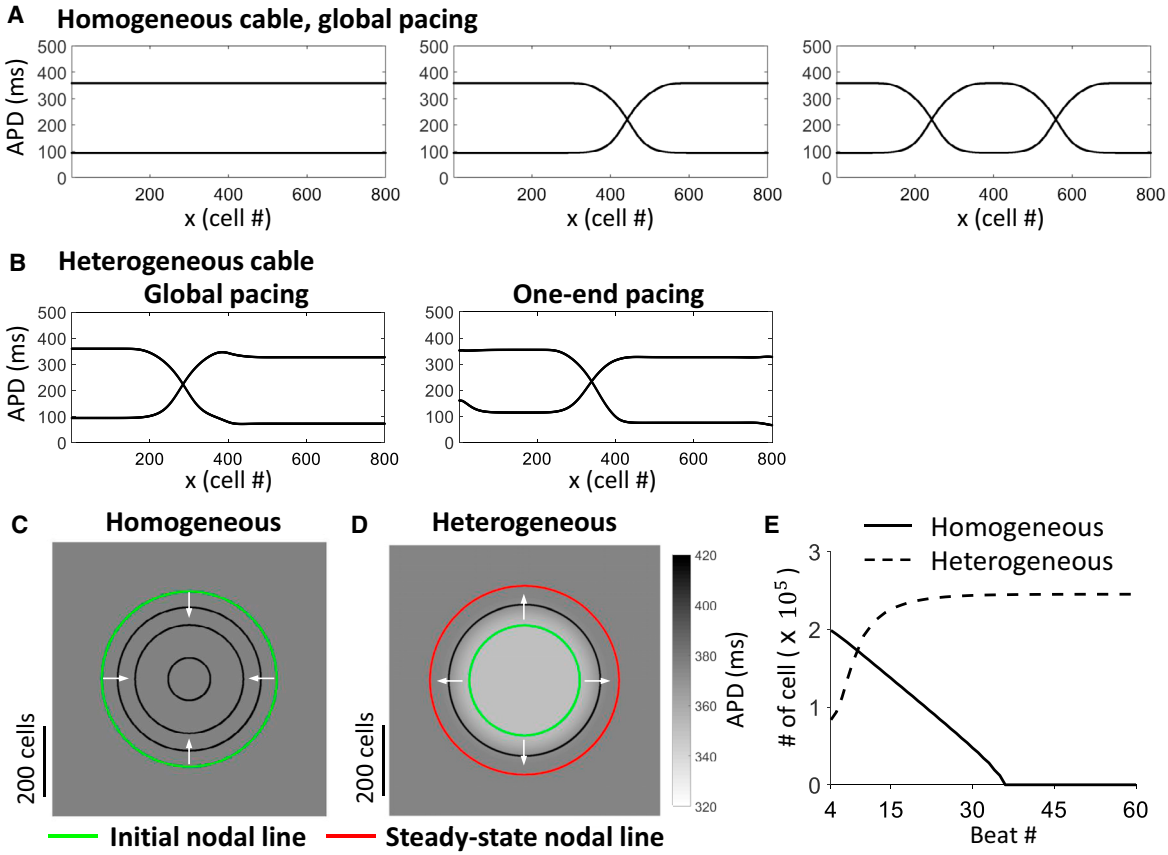

FIGURE 8 SDA formation and nodal ring dynamics for APD alternans induced by I_{to}. (*A*) Initial-condition-induced SCA and SDA in a homogeneous cable with global pacing are shown. PCL = 700 ms. The total number of pacing beats is 500. The left panel shows SCA due to a homogeneous initial condition. The middle panel shows one-node SDA due to the following heterogeneous initial condition: the initial value of the gating variable $x = 0.2$ for the first 400 cells and 0.01 for the next 400 cells. The right panel shows two-node SDA due to the following heterogeneous initial condition: the initial value of the gating variable $x = 0.2$ for the first 200 cells, 0.01 for the next 400 cells, and 0.2 for the last 200 cells. (*B*) SDA induced by two different pacing protocols in a heterogeneous cable with a homogeneous initial condition is shown. Repolarization heterogeneity was modeled by setting $G_K = 0.282$ mS/cm^2 in the first half of the cable and 0.44 mS/cm^2 in the second half. PCL = 700 ms. The total number of pacing beats is 500. The left panel shows global pacing. The right panel shows one-end pacing at the left end of the cable. (*C*) Nodal lines at different time points in a homogeneous 2D tissue show that a heterogeneous initial-condition-induced nodal ring (*green*) shrinks (indicated by *arrows*) and disappears. The initial nodal line was induced using a heterogeneous initial distribution of the gating variable x in a similar way in (*A*). Global pacing with PCL = 700 ms. The tissue size is 800 × 800 cells. (*D*) Nodal lines at different time points in a heterogeneous 2D tissue show that an initial nodal ring expands (indicated by *arrows*) and becomes stable (*red*). The initial nodal line was induced by the repolarization heterogeneity similar to (*B*). The pacing protocol, PCL, and tissue size are the same as in (*C*). Repolarization heterogeneity was modeled by setting $G_K = 0.44$ mS/cm^2 in the center circular region with r = 200 cells and 0.282 mS/cm^2 in the rest of the tissue. The grayscale background in (*C*) and (*D*) is APD under PCL = 2000 ms as indicated by the scale bar. (*E*) The area (total number of cells) inside the ring versus beat number for (*C*) (*solid*) and (*D*) (*dashed*) is shown. To see this figure in color, go online.

In this study, we investigated the formation and stability of SDA induced by heterogeneous initial conditions (including PVCs) or heterogeneous repolarization. It may not be surprising that heterogeneous initial conditions or repolarization can cause out-of-phase alternating (or oscillating) regions. However, a key question to ask is whether the induced SDA is a solution of the spatial system and whether it can remain stable. For example, in the homogeneous cable, because the cells are identical and are diffusively coupled, the heterogeneous initial-condition-induced out-of-phase alternating regions may become synchronized into SCA because of diffusive coupling. Our results show that both SCA and SDA are solutions of the homogeneous cable. For the SDA solutions, the node can be formed anywhere in the cable (Figs. 3*B* and 10 *A*), indicating that the stability of the node is marginal. In cables with repolarization heterogeneities, nodes can be induced by the heterogeneities, but the nodes may not be stable because they may drift from the large alternans region to the small alternans region (see Fig. 5 *B*). However, for either homogeneous or heterogeneous cables, when CVR is engaged (Figs. 2 and 5 *C*), CVR-induced SDA is the only stable solution, and the heterogeneous initial-condition (including PVCs)- and heterogeneity-induced SDA cannot exist.

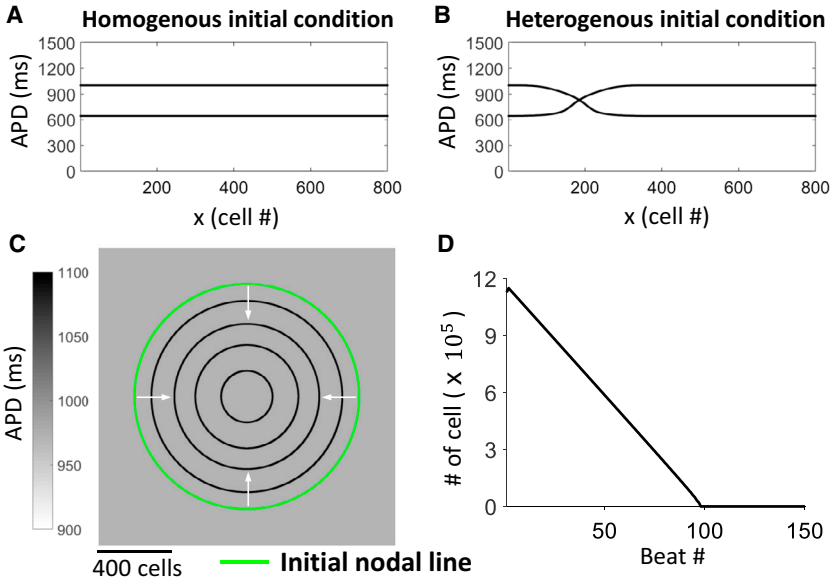

FIGURE 9 SDA formation and nodal ring dynamics for APD alternans induced by EADs at slow heart rates. (*A*) SCA due to homogeneous initial conditions in a homogeneous cable under global pacing is shown. (*B*) SDA induced by a heterogeneous initial condition in the same homogeneous cable as in (*A*) is shown. Heterogeneous initial condition was given by setting $f = 1$ in the first 400 cells and $f = 0.01$ in the next 400 cells at $t = 0$. (*C*) Nodal lines at different time points in a homogeneous 2D tissue show that the initial-condition-induced nodal ring (*green*) shrinks (indicated by *arrows*) and disappears. The gray background is the APD map under PCL = 3000 ms. (*D*) The area (total number of cells) inside the ring versus beat number for the case in (*C*) is shown. Global pacing with PCL = 2500 ms is used for both 1D cable and 2D tissue. For the 1D cable, the total number of pacing beats is 50, and APD from the last two beats is plotted. The 2D tissue size is 1600 × 1600 cells. To see this figure in color, go online.

In 2D tissue, because of the neutral stability properties of the SDA nodes, curved nodal lines cannot exist in homogeneous tissue because the tension generated by the curvature causes the node lines to move until they become straight or disappear (Figs. 6 and 7). However, the tension generated by the curvature of the nodal line and the one generated by the heterogeneity may match properly (against each other) to result in stable nodal lines in 2D tissue. Again, when CVR is engaged, the CVR-induced SDA is the only stable solution, and the nodal lines do not depend on the structure of the heterogeneities (see Fig. 7 *B*).

Therefore, in the absence of CVR, marginally stable SDA with straight nodal lines can occur in homogeneous tissue. Stable SDA can occur in cardiac tissue in the presence of repolarization heterogeneities. This may account for the SDA observed in experiments (20–22) that cannot be explained by the CVR-induced mechanism of SDA. The mechanism of SDA formation investigated in this study may also have important implications for cardiac arrhythmogenesis in the human heart as discussed below.

Note that heterogeneous initial-condition-induced SDA may not occur in real life. This is because the heart is continuously beating from the beginning of life, driven by the electrical signal originating from the sinus node; thus, there are no such initial condition heterogeneities. However, the symmetry of concordance may be broken by PVCs or pre-existing repolarization heterogeneities as shown in our simulations, which is equivalent to heterogeneous initial conditions.

Implications for cardiac arrhythmogenesis

The important role of SDA in cardiac arrhythmogenesis is that it generates a large repolarization gradient. This large gradient can provide not only a substrate for conduction block (8,9,65) but also a tissue state for the genesis of

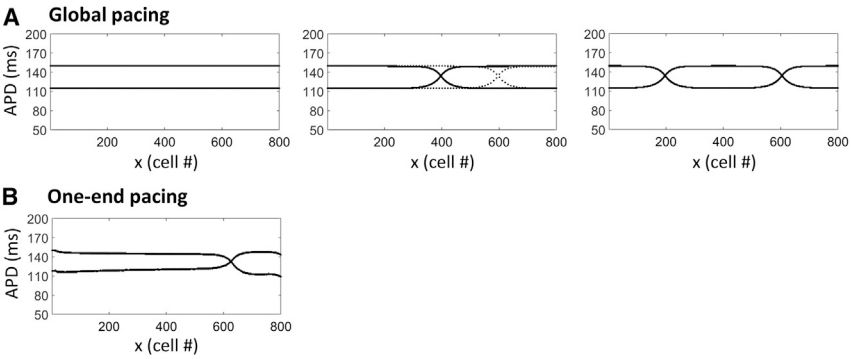

FIGURE 10 SDA formation in a homogeneous cable with the rabbit ventricular action potential model. The parameters are the same as in the original model. PCL = 180 ms and the total number of pacing beat is 50. APD from the last two beats is plotted for each case. (*A*) SDA formation with global pacing is shown. The left panel shows homogeneous initial condition. The middle panel shows one-node SDA induced by heterogeneous initial conditions. Solid lines and dashed lines are from two different initial conditions. The right panel shows a two-node SDA induced by a heterogeneous initial condition. Heterogeneous initial conditions were set by heterogeneous distributions of a gating variable of the slow component of delayed rectifier K^+ current. (*B*) SDA induced by one-end pacing with a homogenous initial condition is shown.

PVCs (39). SDA may underlie T-wave polarity alternans in the electrocardiograms, which is widely observed in clinical settings (66–68). Moreover, CVR-induced SDA may also lead to concomitant QRS alternans (8,9). The mechanism of CVR-induced SDA may occur under the following conditions: 1) fast pacing in electrophysiological studies or during tachycardia, in which the heart rates are fast enough to engage CVR, 2) fast or normal heart rates under the condition of ischemia in which the Na^+ channel recovery is slowed so that the CV varies in a wide range of DI (49), and 3) fast or normal heart rates under LQTS, in which APD is substantially lengthened so that the DI is short.

However, CVR-induced SDA may not be responsible for T-wave polarity alternans under the following conditions: 1) if many of the T-wave polarity alternans observed in patients occur at normal or slow heart rates (66–68), in which the DI may be too large to engage CVR, and 2) if T-wave polarity alternans is solely due to SDA occurring in the cardiac layers (i.e., from the endocardial layer to the epicardial layer) even if the heart rate is fast or the DI is short. Under the second condition, no conduction occurs within the layers because they are transverse to the transmural direction along which normal sinus conduction occurs, similar to the global pacing used in this study. Therefore, SDA and thus T-wave polarity alternans under these conditions may be caused by repolarization heterogeneities, the mechanism of SDA investigated in our study.

Limitations

In this study, we mainly used the LR1 model, in which APD alternans are purely voltage-driven alternans. Because this model lacks intracellular Ca^{2+} cycling, it cannot be used for investigating Ca^{2+}-driven alternans. Although the alternans dynamics in the rabbit ventricular model depend on both voltage and Ca^{2+} cycling dynamics (44) and we observed similar spatiotemporal alternans dynamics (Fig. 10), it needs to be investigated whether the same spatiotemporal alternans dynamics still hold when alternans is purely Ca^{2+} driven. We used two simple pacing protocols in simple 1D and 2D tissue models, but a heart is a 3D organ with complex structural and electrophysiological heterogeneities. Therefore, the excitation and conduction in the heart may be much more complex, in which the tensions generated by CVR, curvature, and heterogeneities will compete or cooperate to determine the SDA nodal line/surface structure and dynamics. Finally, this study is a computer simulation study; thus, more rigorous analyses are still needed to better understand the mechanisms of the node or nodal line dynamics, such as the minimal distance between two neighboring nodes in a multinode SDA, the relationship between curvature and nodal line movement, and the node drift dynamics in a heterogeneous tissue. Nevertheless, our study provides a basic understanding of the roles of CVR, nodal line curvature, and repolarization heterogeneities in SDA formation and dynamics in cardiac tissue.

CONCLUSIONS

Our simulation results show that SDA can occur in cardiac tissue either in the presence or absence of CVR. CVR-induced SDA only occurs at fast heart rates or when CVR is broadened. Non-CVR-induced SDA can occur at any heart rate, but its formation and stability depends on pacing protocols and repolarization heterogeneities. Both mechanisms of SDA may occur in patients under different clinical conditions.

SUPPORTING MATERIAL

Supporting Material can be found online at https://doi.org/10.1016/j.bpj.2020.02.008.

AUTHOR CONTRIBUTIONS

C.H. performed the simulations. C.H., Z.S., and J.L. contributed to the design of the study. Z.Q. conceived and designed the overall research. C.H., Z.S., J.L., and Z.Q. analyzed data. Z.S. and Z.Q. wrote the article. All authors edited the article.

ACKNOWLEDGMENTS

This study is supported by National Institutes of Health grants R01 HL134709, R01 HL139829, and F30 HL140864. C.H. is supported by grants from the China Scholarship Council and the National Natural Science Foundation of China (grant no. 11775020).

REFERENCES

1. Traube, L. 1872. Ein fall von pulsus bigeminus nebst bemerkungen tiber die lebershwellungen bei klappenfehlern und uber acute leberatrophic. *Ber. Klin. Wschr.* 9:185.
2. Rosenbaum, D. S. 2001. T wave alternans: a mechanism of arrhythmogenesis comes of age after 100 years. *J. Cardiovasc. Electrophysiol.* 12:207–209.
3. Armoundas, A. A., G. F. Tomaselli, and H. D. Esperer. 2002. Pathophysiological basis and clinical application of T-wave alternans. *J. Am. Coll. Cardiol.* 40:207–217.
4. Qu, Z., and J. N. Weiss. 2015. Mechanisms of ventricular arrhythmias: from molecular fluctuations to electrical turbulence. *Annu. Rev. Physiol.* 77:29–55.
5. Narayan, S. M. 2006. T-wave alternans and the susceptibility to ventricular arrhythmias. *J. Am. Coll. Cardiol.* 47:269–281.
6. Moore, P. K., K. E. Raffel, and I. R. Whitman. 2017. Macroscopic T-wave alternans: a red flag for code blue. *JAMA Intern. Med.* 177:1520–1522.
7. Cao, J. M., Z. Qu, …, P. S. Chen. 1999. Spatiotemporal heterogeneity in the induction of ventricular fibrillation by rapid pacing: importance of cardiac restitution properties. *Circ. Res.* 84:1318–1331.
8. Pastore, J. M., S. D. Girouard, …, D. S. Rosenbaum. 1999. Mechanism linking T-wave alternans to the genesis of cardiac fibrillation. *Circulation.* 99:1385–1394.

9. Qu, Z., A. Garfinkel, …, J. N. Weiss. 2000. Mechanisms of discordant alternans and induction of reentry in simulated cardiac tissue. *Circulation.* 102:1664–1670.
10. Walker, M. L., and D. S. Rosenbaum. 2003. Repolarization alternans: implications for the mechanism and prevention of sudden cardiac death. *Cardiovasc. Res.* 57:599–614.
11. Choi, B. R., W. Jang, and G. Salama. 2007. Spatially discordant voltage alternans cause wavebreaks in ventricular fibrillation. *Heart Rhythm.* 4:1057–1068.
12. Qu, Z., Y. Xie, …, J. N. Weiss. 2010. T-wave alternans and arrhythmogenesis in cardiac diseases. *Front. Physiol.* 1:154.
13. Muñoz, L. M., A. R. M. Gelzer, …, N. F. Otani. 2018. Discordant alternans as a mechanism for initiation of ventricular fibrillation in vitro. *J. Am. Heart Assoc.* 7:e007898.
14. Watanabe, M. A., F. H. Fenton, …, A. Karma. 2001. Mechanisms for discordant alternans. *J. Cardiovasc. Electrophysiol.* 12:196–206.
15. Echebarria, B., and A. Karma. 2002. Instability and spatiotemporal dynamics of alternans in paced cardiac tissue. *Phys. Rev. Lett.* 88:208101.
16. Hayashi, H., Y. Shiferaw, …, Z. Qu. 2007. Dynamic origin of spatially discordant alternans in cardiac tissue. *Biophys. J.* 92:448–460.
17. de Diego, C., R. K. Pai, …, M. Valderrábano. 2008. Spatially discordant alternans in cardiomyocyte monolayers. *Am. J. Physiol. Heart Circ. Physiol.* 294:H1417–H1425.
18. Mironov, S., J. Jalife, and E. G. Tolkacheva. 2008. Role of conduction velocity restitution and short-term memory in the development of action potential duration alternans in isolated rabbit hearts. *Circulation.* 118:17–25.
19. Banville, I., and R. A. Gray. 2002. Effect of action potential duration and conduction velocity restitution and their spatial dispersion on alternans and the stability of arrhythmias. *J. Cardiovasc. Electrophysiol.* 13:1141–1149.
20. Gizzi, A., E. M. Cherry, …, F. H. Fenton. 2013. Effects of pacing site and stimulation history on alternans dynamics and the development of complex spatiotemporal patterns in cardiac tissue. *Front. Physiol.* 4:71.
21. Ziv, O., E. Morales, …, B. R. Choi. 2009. Origin of complex behaviour of spatially discordant alternans in a transgenic rabbit model of type 2 long QT syndrome. *J. Physiol.* 587:4661–4680.
22. Lau, E., K. Kossidas, …, B. R. Choi. 2015. Spatially discordant alternans and arrhythmias in tachypacing-induced cardiac myopathy in transgenic LQT1 rabbits: the importance of IKs and Ca2+ cycling. *PLoS One.* 10:e0122754.
23. Christini, D. J., M. L. Riccio, …, R. F. Gilmour, Jr. 2006. Control of electrical alternans in canine cardiac purkinje fibers. *Phys. Rev. Lett.* 96:104101.
24. Drew, B. J., M. J. Ackerman, …, W. Zareba; American Heart Association Acute Cardiac Care Committee of the Council on Clinical Cardiology, the Council on Cardiovascular Nursing, and the American College of Cardiology Foundation. 2010. Prevention of torsade de pointes in hospital settings: a scientific statement from the American Heart Association and the American College of Cardiology Foundation. *Circulation.* 121:1047–1060.
25. Zareba, W., A. J. Moss, …, W. J. Hall. 1994. T wave alternans in idiopathic long QT syndrome. *J. Am. Coll. Cardiol.* 23:1541–1546.
26. Wegener, F. T., J. R. Ehrlich, and S. H. Hohnloser. 2008. Amiodarone-associated macroscopic T-wave alternans and torsade de pointes unmasking the inherited long QT syndrome. *Europace.* 10:112–113.
27. Ariyarajah, V., H. Smith, …, A. Khadem. 2008. Spontaneous alternans in Brugada ST-segment morphology within minutes. *J. Electrocardiol.* 41:302–305.
28. Fazelifar, A. F., M. Haghjoo, …, M. A. Sadr-Ameli. 2006. Spontaneous alternans in Brugada ECG morphology. *J. Interv. Card. Electrophysiol.* 15:131–134.
29. Morita, H., S. Nagase, …, T. Ohe. 2002. Spontaneous T wave alternans and premature ventricular contractions during febrile illness in a patient with Brugada syndrome. *J. Cardiovasc. Electrophysiol.* 13:816–818.
30. Morita, H., D. P. Zipes, …, J. Wu. 2006. T wave alternans in an in vitro canine tissue model of Brugada syndrome. *Am. J. Physiol. Heart Circ. Physiol.* 291:H421–H428.
31. Omichi, C., N. Fujimoto, …, A. Kasai. 2010. Ischemia-induced Brugada-type ST-segment alternans and Brugada syndrome. *Int. J. Cardiol.* 144:429–430.
32. Zhou, Y., J. Wang, …, Y. Wang. 2013. ST-T-wave alternans in Brugada electrocardiogram type I pattern during the resolution of febrile states. *Cardiovasc. J. Afr.* 24:e1–e3.
33. Holley, C. L., and J. A. Cooper. 2009. Macrovolt T-wave alternans and polymorphic ventricular tachycardia. *Circulation.* 120:445–446.
34. Chow, T., D. J. Kereiakes, …, P. S. Chan. 2006. Prognostic utility of microvolt T-wave alternans in risk stratification of patients with ischemic cardiomyopathy. *J. Am. Coll. Cardiol.* 47:1820–1827.
35. Sato, D., Y. Shiferaw, …, A. Karma. 2006. Spatially discordant alternans in cardiac tissue: role of calcium cycling. *Circ. Res.* 99:520–527.
36. Landaw, J., and Z. Qu. 2018. Memory-induced nonlinear dynamics of excitation in cardiac diseases. *Phys. Rev. E.* 97:042414.
37. Hopenfeld, B. 2006. Mechanism for action potential alternans: the interplay between L-type calcium current and transient outward current. *Heart Rhythm.* 3:345–352.
38. Sato, D., L. H. Xie, …, Z. Qu. 2009. Synchronization of chaotic early afterdepolarizations in the genesis of cardiac arrhythmias. *Proc. Natl. Acad. Sci. USA.* 106:2983–2988.
39. Liu, W., T. Y. Kim, …, Z. Qu. 2018. Mechanisms linking T-wave alternans to spontaneous initiation of ventricular arrhythmias in rabbit models of long QT syndrome. *J. Physiol.* 596:1341–1355.
40. Liu, M. B., N. Vandersickel, …, Z. Qu. 2019. R-from-T as a common mechanism of arrhythmia initiation in long QT syndromes. *Circ Arrhythm Electrophysiol.* 12:e007571.
41. Nivala, M., Z. Song, …, Z. Qu. 2015. T-tubule disruption promotes calcium alternans in failing ventricular myocytes: mechanistic insights from computational modeling. *J. Mol. Cell. Cardiol.* 79:32–41.
42. Qu, Z., M. B. Liu, and M. Nivala. 2016. A unified theory of calcium alternans in ventricular myocytes. *Sci. Rep.* 6:35625.
43. Luo, C. H., and Y. Rudy. 1991. A model of the ventricular cardiac action potential. Depolarization, repolarization, and their interaction. *Circ. Res.* 68:1501–1526.
44. Mahajan, A., Y. Shiferaw, …, J. N. Weiss. 2008. A rabbit ventricular action potential model replicating cardiac dynamics at rapid heart rates. *Biophys. J.* 94:392–410.
45. Jordan, P. N., and D. J. Christini. 2006. Action potential morphology influences intracellular calcium handling stability and the occurrence of alternans. *Biophys. J.* 90:672–680.
46. Zhu, Z. I., and C. E. Clancy. 2007. L-type Ca2+ channel mutations and T-wave alternans: a model study. *Am. J. Physiol. Heart Circ. Physiol.* 293:H3480–H3489.
47. Zhou, X., A. Bueno-Orovio, …, B. Rodriguez. 2016. In vivo and in silico investigation into mechanisms of frequency dependence of repolarization alternans in human ventricular cardiomyocytes. *Circ. Res.* 118:266–278.
48. Prudat, Y., R. V. Madhvani, …, J. P. Kucera. 2016. Stochastic pacing reveals the propensity to cardiac action potential alternans and uncovers its underlying dynamics. *J. Physiol.* 594:2537–2553.
49. Qu, Z., H. S. Karagueuzian, …, J. N. Weiss. 2004. Effects of Na(+) channel and cell coupling abnormalities on vulnerability to reentry: a simulation study. *Am. J. Physiol. Heart Circ. Physiol.* 286:H1310–H1321.
50. Lukas, A., and C. Antzelevitch. 1993. Differences in the electrophysiological response of canine ventricular epicardium and endocardium to ischemia. Role of the transient outward current. *Circulation.* 88:2903–2915.
51. Maoz, A., T. Krogh-Madsen, and D. J. Christini. 2009. Instability in action potential morphology underlies phase 2 reentry: a mathematical modeling study. *Heart Rhythm.* 6:813–822.

52. Cantalapiedra, I. R., A. Peñaranda, …, B. Echebarria. 2009. Reexcitation mechanisms in epicardial tissue: role of I(to) density heterogeneities and I(Na) inactivation kinetics. *J. Theor. Biol.* 259:850–859.

53. Xie, Y., A. Garfinkel, …, Z. Qu. 2009. Cardiac alternans induced by fibroblast-myocyte coupling: mechanistic insights from computational models. *Am. J. Physiol. Heart Circ. Physiol.* 297:H775–H784.

54. Landaw, J., A. Garfinkel, …, Z. Qu. 2017. Memory-induced chaos in cardiac excitation. *Phys. Rev. Lett.* 118:138101.

55. Guo, D., Y. Wu, …, G.-X. Yan. 2008. Abstract 5335: discordant T wave and mechanical alternans in left ventricular hypertrophy: role of late sodium current. *Circulation.* 118:S529–S530.

56. Guo, D., L. Young, …, G. X. Yan. 2008. Calcium-activated chloride current contributes to action potential alternations in left ventricular hypertrophy rabbit. *Am. J. Physiol. Heart Circ. Physiol.* 295:H97–H104.

57. Sato, D., L. H. Xie, …, Z. Qu. 2010. Irregularly appearing early afterdepolarizations in cardiac myocytes: random fluctuations or dynamical chaos? *Biophys. J.* 99:765–773.

58. Qu, Z., and D. Chung. 2012. Mechanisms and determinants of ultralong action potential duration and slow rate-dependence in cardiac myocytes. *PLoS One.* 7:e43587.

59. Liu, T., C. Patel, …, G.-X. Yan. 2013. Abstract 10368: early afterdepolarization alternans manifests T wave alternans in left ventricular hypertrophy. *Circulation.* 128:A10368.

60. Fox, J. J., M. L. Riccio, …, R. F. Gilmour, Jr. 2002. Spatiotemporal transition to conduction block in canine ventricle. *Circ. Res.* 90:289–296.

61. Qu, Z. 2004. Dynamical effects of diffusive cell coupling on cardiac excitation and propagation: a simulation study. *Am. J. Physiol. Heart Circ. Physiol.* 287:H2803–H2812.

62. Echebarria, B., and A. Karma. 2007. Amplitude equation approach to spatiotemporal dynamics of cardiac alternans. *Phys. Rev. E Stat. Nonlin. Soft Matter Phys.* 76:051911.

63. Sato, D., D. M. Bers, and Y. Shiferaw. 2013. Formation of spatially discordant alternans due to fluctuations and diffusion of calcium. *PLoS One.* 8:e85365.

64. Shiferaw, Y., G. L. Aistrup, and J. A. Wasserstrom. 2018. Synchronization of triggered waves in atrial tissue. *Biophys. J.* 115:1130–1141.

65. Qu, Z., A. Garfinkel, and J. N. Weiss. 2006. Vulnerable window for conduction block in a one-dimensional cable of cardiac cells, 1: single extrasystoles. *Biophys. J.* 91:793–804.

66. Cruz Filho, F. E., I. G. Maia, …, J. C. Ribeiro. 2000. Electrical behavior of T-wave polarity alternans in patients with congenital long QT syndrome. *J. Am. Coll. Cardiol.* 36:167–173.

67. Schwartz, P. J., L. Crotti, and R. Insolia. 2012. Long-QT syndrome: from genetics to management. *Circ Arrhythm Electrophysiol.* 5:868–877.

68. Pérez-Riera, A. R., R. Barbosa-Barros, …, L. C. de Abreu. 2018. The congenital long QT syndrome type 3: an update. *Indian Pacing Electrophysiol. J.* 18:25–35.